One-step synthesis of graphene hollow nanoballs with various nitrogen-doped states for electrocatalysis in dye-sensitized solar cells

Chi-Ang Tseng [a, 1], Chuan-Pei Lee [b, 1], Yi-June Huang [c], Hao-Wei Pang [c], Kuo-Chuan Ho [c, d, **], Yit-Tsong Chen [a, b, *]

[a] Department of Chemistry, National Taiwan University, No. 1, Sec. 4, Roosevelt Road, Taipei 106, Taiwan
[b] Institute of Atomic and Molecular Sciences, Academia Sinica, P.O. Box 23-166, Taipei 106, Taiwan
[c] Department of Chemical Engineering, National Taiwan University, Taipei 106, Taiwan
[d] Institute of Polymer Science and Engineering, National Taiwan University, Taipei 106, Taiwan

ARTICLE INFO

ABSTRACT

Nitrogen-doped graphene hollow nanoballs (N-GHBs) were synthesized in chemical vapor deposition (CVD) reaction using melamine as a chemical precursor via an *in situ* nitrogen-doping approach. In the CVD reaction, N-GHBs were deposited directly on carbon cloth (CC) to be used as an efficient metal-free electrocatalyst for dye-sensitized solar cell (DSSC) applications. The highly curved N-GHBs could avoid the self-assembly restacking of planar graphene sheets, which usually occurred during the film preparation. Keeping oxygen contaminations from N-GHBs, the characteristic electrical conductivity of graphene was preserved in the as-synthesized N-GHBs. By controlling the evaporation temperature of melamine, the nitrogen-doping content of 8.7—14.0% and different nitrogen-doped configurations in N-GHBs could be adjusted. The catalytic activities of different nitrogen-doped states in N-GHBs toward the triiodide (I_3^-) reduction in DSSCs were investigated, revealing that the pyridinic and quaternary nitrogens, rather than the total nitrogen doping level, in N-GHBs are mainly responsible for their catalytic activities in DSSCs. For solar cell applications, the high surface area and heteroatomic nitrogens of GHBs can remarkably improve the catalytic activity toward the triiodide reduction, lower the charge-transfer resistance, and enhance the corresponding photovoltaic performance (7.53%), which is comparable to that (7.70%) of a standard sputtered Pt counter electrode-based cell. These exceptional properties allow N-GHBs/CC to act as a promising electrocatalytic electrode for DSSC and other electrochemical energy applications.

© 2018 Elsevier Ltd. All rights reserved.

1. Introduction

Dye-sensitized solar cells (DSSCs) have drawn widespread attention in solar energy markets due to their high conversion efficiency, low cost, flexibility and light weight, and simple fabrication processes [1,2]. A DSSC comprises three main components of a dye-sensitized titania (TiO_2) photoanode, the triiodide/iodide (I^-/I_3^-) electrolyte, and a platinum (Pt)/fluorine-doped tin oxide (FTO) counter electrode (CE); in particular, CE plays a crucial role in

the charge balance of electrolytes. The Pt and FTO used for the CE of traditional DSSCs are attributed to their excellent catalytic activity and high electrical conductivity, respectively. However, the scarcity and poor iodide corrosion-resistance of Pt together with the rigidity and heavy weight of FTO have restricted their commercial applications [3—5]. Therefore, searching for alternative candidates, such as carbon-based materials, transition-metal compounds, and conducting polymers, has been extensively proceeded. Among them, carbon-based materials, including graphene, activated carbons, carbon blacks, and carbon nanotubes, are very promising substituents because of their low cost, good catalytic ability, high conductivity, and high chemical stability in corrosive electrolytes [6,7].

Graphene, a two-dimensional (2D) atomically thick carbon material, has been highlighted for its high conductivity, good transparency, and large specific surface area [8—10]. However,

---

* Corresponding author. Department of Chemistry, National Taiwan University, No. 1, Sec. 4, Roosevelt Road, Taipei 106, Taiwan.
** Corresponding author. Department of Chemical Engineering, National Taiwan University, Taipei 106, Taiwan.
E-mail addresses: kcho@ntu.edu.tw (K.-C. Ho), ytcchem@ntu.edu.tw (Y.-T. Chen).
[1] These authors contributed equally.

pristine graphene shows poor catalytic ability toward the triiodide (I_3^-) reduction in DSSC, because the active sites exist only at the edges of graphene. To address this issue, the insertion of heteroatoms into the basal plane of graphene and the structural engineering of graphene to three-dimensional (3D) shape/morphology are efficient routes for increasing active sites and catalytic ability. Several reports have shown great promises for the triiodide reduction via the chemical doping of graphene with heteroatoms, such as nitrogen [11–13], sulfur [14,15], oxygen [16], and phosphorous [17]. Among these dopants, the introduction of nitrogen into graphene not only creates an electron-donating area to enhance the iodine adsorption [18], but also increases the conjugation between the lone-pair electrons of nitrogen and the delocalized π-system of graphene, resulting in an enhancement of the electrocatalytic reactivity in DSSCs.

In addition, an increase of the catalytic activity of CEs can also be achieved by the structural transformation of graphene, such as N-doped nanoplatelets [19], N-doped graphene foams [20], and N-doped graphene/carbon nanotube 3D structures [21]. It is well known that both high surface area and good electrical conductivity are prerequisite for a promising CE material. However, most of the N-doped graphenes were derived from reduced graphene oxides (rGO), which suffered from their inclination to restacking in the structural formation and low conductivity in the electrical performance [22], leading to a decrease of the accessible active sites and an increase of the total internal resistance in DSSC. Moreover, a quantity of residual oxygen-containing functional groups could still remain in the nitrogen-doped rGO samples during the nitrogen-doping process due to the difficulty of completely eliminating oxygen-containing groups by thermal annealing. These residual oxygen-containing groups in nitrogen-doped rGO could also contribute to catalytic activity for the triiodide reduction, making it difficult to evaluate the role of N-doped species toward the triiodide reduction reaction. Recent reports showed that several nitrogen-doped states, e.g., pyridinic N, pyrrolic N, quaternary N, and pyridinic N-oxide, always coexist in nitrogen-doped graphene and not all of these nitrogen-doped configurations contribute to catalytic activity [23]. Therefore, the investigation of individual N-doped states toward catalytic activities is highly demanded to maximize the performance of a nitrogen-doped graphene CE in DSSCs.

Here, we developed a one-step chemical vapor deposition (CVD, Fig. 1a) method to synthesize nitrogen-doped graphene hollow nanoballs (N-GHBs) directly on carbon cloth (referred to as N-GHBs/CC) for the uses of an all-carbon CE in DSSCs. In this one-step CVD synthesis, the melamine molecule (i.e., 1,3,5-triazine-2,4,6-triamine with its chemical structure shown in Fig. 1a) was selected as a chemical precursor for the carbon and nitrogen sources in high-temperature CVD reaction, where the versatile fragments containing C−N and C=N groups from the decomposed melamine could rearrange to facilitate the N-doped graphene formation. The curved structure of the as-synthesized N-GHBs has the advantages of preventing the restacking of graphene layers that usually occurred during the film preparation, maximizing the surface area to enhance charge transfers, and maintaining the electrical conductivity for high electrochemical performance. Furthermore, by analyzing different N-doped configurations and their contents in the N-GHB samples, we realized that the pyridinic N and quaternary N states (as illustrated in Fig. 1b) act as active sites to enhance the triiodide reduction and play a significant electrocatalytic role in DSSCs. As a result, a DSSC device with the N-GHBs/CC-fabricated CE exhibited a high power conversion efficiency (PCE) of 7.53%, which is comparable to 7.70% of a sputtered Pt/CC CE-based cell.

2. Results and discussion

The CVD apparatus used for the growth of N-GHBs on CC is illustrated in Fig. 1a with the experimental procedures described in the Supporting Information. In N-GHBs, the heteroatomic N could have three bonding configurations within the carbon lattice (Fig. 1b), including pyridinic N, quaternary N, and pyrrolic N. While a pyridine N (pyrrolic N) has a substitutional N atom bonding to two C atoms in the six-membered (five-membered) N-containing aromatic rings, a quaternary N replaces a C atom in the carbon framework, which bonds to three neighboring C atoms and is located at the basal plane of a graphene layer.

In the CVD synthesis of N-GHBs, we found that the ratios of pyridinic N, quaternary N, and pyrrolic N in the as-produced N-GHB samples could be controlled by varying the evaporation temperature of melamine, which was achieved by placing the melamine precursor at different locations to the furnace. As illustrated in
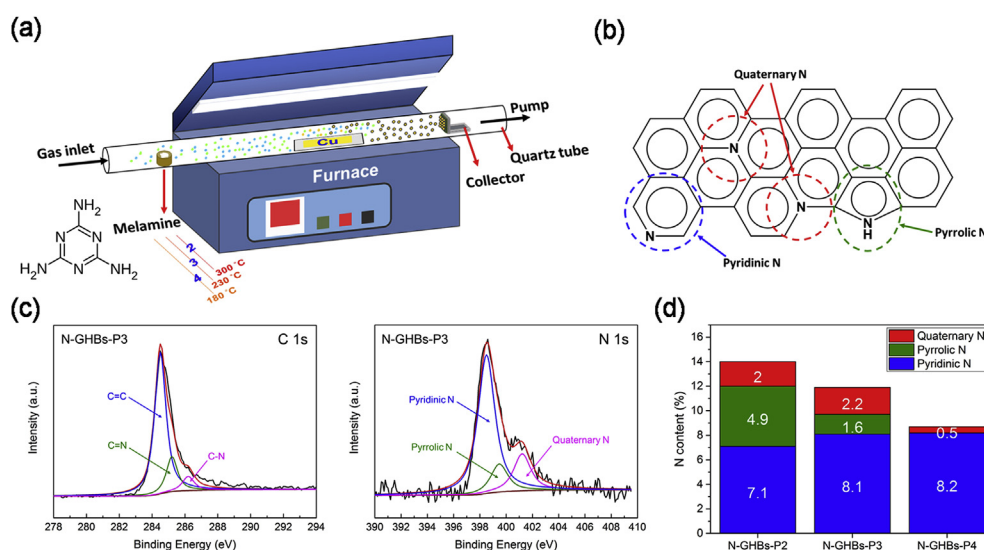

Fig. 1. (a) A schematic representation of the CVD design for the growth of N-GHBs. (b) Three types of the N-doped states in N-GHBs include pyridinic N, pyrrolic N, and quaternary N. (c) High-resolution XPS spectra of C1s and N1s in an N-GHBs-P3 sample. (d) A distribution of various N-doped states in different N-GHBs samples.

Fig. 1a, the N-GHBs-P2, N-GHBs-P3, and N-GHBs-P4 products were obtained by locating the melamine precursor at 2, 3, and 4 cm away from the furnace inlet with their local temperatures of 300, 230, and 180 °C, respectively. Various chemical bonds in the as-produced N-GHBs were characterized by X-ray photoelectron spectroscopy (XPS) as shown in Fig. 1c and Figure S1 of the Supporting Information. The high-resolution C1s and N1s spectra of the N-GHBs-P3 sample (Fig. 1c) reveal the characteristic chemical bonds of C=C at 284.5 eV, C=N at 285.1 eV, and C–N at 286.2 eV [24,25], indicating that the graphite-like sp^2 carbon is dominant and the heteroatomic N is successfully incorporated into the graphene lattice. More importantly, the deconvoluted XPS N1s spectrum (Fig. 1c) manifests different N-doped states (pyridinic N at 398.5 eV, pyrrolic N at 399.5 eV, and quaternary N at 401.2 eV) and their contents in the N-GHBs-P3 sample [26,27]. Similar to the spectral analysis for the XPS spectra of N-GHBs-P3 (Fig. 1c), those of N-GHBs-P2 and N-GHBs-P4 are shown in Figure S1 of the Supporting Information and the distributions of different N-doped states in these three samples are summarized in Fig. 1d.

It is noted that melamine could be evaporated faster at higher reaction temperature; thus more nitrogen source could supply in the CVD chamber. By adjusting the location/temperature of melamine (Fig. 1a), the N-doping contents in the three N-GHB samples were modulated from 8.7 to 14.0% (Fig. 1d). Such high N-doping contents in N-GHBs are attributed to the plentiful edges of the highly curved GHB structure to accommodate N atoms in the *in situ* N-doping process. It is well known that the pyrrolic N is less thermally stable, as compared to pyridinic N and quaternary N, under such high synthetic temperature (i.e., 1090 °C) [28]. On the other hand, the formation of quaternary N requires much higher energy than the other two N-doped states due to the involvement of a substitutional reaction [29]; besides the highly-curved structure of GHBs consists of many nano-sized crystalline graphene (~10 nm in size; see Figure S2) and provides only limited graphene basal plane for quaternary N formation. Accordingly, the pyridinic N becomes the dominant configuration in all N-GHB samples (Fig. 1d) [30]. With a less supply of melamine (i.e., by decreasing the evaporation temperature), pyrrolic N dramatically decreased due to its thermal instability and even disappeared in the case of the lowest melamine supply (i.e., N-GHBs-P4). Moreover, the contents of quaternary N kept almost the same under the highest and moderate melamine supplies (i.e., N-GHBs-P3 and N-GHBs-P2), but significantly decreased at the lowest melamine supply (i.e., N-GHBs-P4), indicating that the insufficient nitrogen source also limited the formation of quaternary N.

In a previous study, Lin et al. [11] demonstrated that the charge-transfer resistance of a Pt/FTO substrate could be reduced by adding nitrogen-doped graphene sheets because of the formation of an extended electron-transfer surface [31]. For our synthesized GHBs/CC and N-GHBs/CC, the scanning electron microscopy (SEM) images of the well-distributed GHBs (Fig. 2a) and N-GHBs (Fig. 2b) on CC show an extensive surface for efficient charge transfers toward the triiodide reduction in DSSCs. The energy dispersive elemental mappings of C (Fig. 2c) and N (Fig. 2d) in an N-GHBs/CC further confirm the uniform distribution of N-dopants in the C framework of the N-GHBs/CC. With the structural analyses by electron microscopy, a TEM image (Fig. 2e) demonstrates that N-GHBs possess the hollow spherical structure and an HRTEM image (Fig. 2f) reveals that the spherical graphitic layers are interrupted and defective [32] with the thickness of ~3.5 nm corresponding to ~10 layers of graphene. The interrupted and defective graphitic layers of N-GHBs could be attributed to the spherical structure with substitutional N atoms [33], where the interplanar spacing of ~3.4 Å also consists with the layer-to-layer separation in multi-layered graphene.

In a DSSC, the photo-excited electrons in the dye molecules inject into the conducting band of a TiO_2 photoanode; meanwhile, while the oxidized dye can be reduced back by the I^- ions in electrolyte, the resultant I_3^- ions are reduced at the CE ($I_3^- + 2e^- \rightarrow 3I^-$). As a consequence, the reduction reaction of I_3^- at CE plays an important role to maintain the steady power output of a DSSC [34]. To investigate the electrocatalytic activities and reaction kinetics of the as-prepared N-GHBs/CC electrodes for the I^-/I_3^- redox reaction, the cyclic voltammogram was performed (Fig. 3), in which the higher cathodic peak current density (J_{PC}) represents the better apparent electrocatalytic activity for the I_3^- reduction and the peak separation (ΔE_P; i.e., the potential difference between the oxidation and reduction peaks) varies inversely with the intrinsic heterogeneous charge-transfer rate constant ($k°$) [24,35,36].

Fig. 3 shows the cyclic voltammograms and corresponding electrochemical parameters of different N-GHBs/CC electrodes. The N-GHBs-P4/CC electrode with the lowest N/C ratio (8.70%, in Fig. 1d) exhibits the smallest J_{PC} (−1.36 mA cm^{-2}) and the largest ΔE_P (660 mV) among the N-GHBs/CC electrodes tested. For N-GHBs-P3/CC, as the N/C ratio increased to 12.1% (Fig. 1d), the J_{PC} was enhanced to −1.68 mA cm^{-2} but the ΔE_P was reduced significantly to 550 mV. However, with a further increase of the N/C ratio to 14.0% (i.e., N-GHBs-P2/CC), the J_{PC} decreased (to −1.55 mA cm^{-2}) but the ΔE_P increased slightly (to 570 mV). This outcome implies that the catalytic ability of N-GHBs could not be improved by simply increasing the N/C ratio. Interestingly, with different N-doped states in the N-GHB samples analyzed in Fig. 1d, we found that the total contents of pyridinic N and quaternary N have a high positive correlation with the catalytic ability of N-GHBs. Accordingly, the N-GHBs-P3/CC electrode, which has the highest amounts of pyridinic N and quaternary N, relative to the other two electrodes tested, possesses the largest J_{PC} and smallest ΔE_P. This result is well consistent with the recent reports [24,30,37] that some special N-functionalized groups, like pyridinic N and quaternary N, on the graphene plane play the most important roles for catalytic reaction, in sharp contrast to other groups with negligible contributions, such as pyrrolic N and pyridinic N-oxide rings. Consequently, the best N-GHBs/CC electrode, i.e., N-GHBs-P3/CC, was selectively used as an all-carbon CE for further investigation of the photovoltaic performance in DSSCs.

Fig. 4a shows the photocurrent density vs. voltage ($J-V$) curves of the DSSCs using various CEs of bare CC, GHBs/CC, N-GHBs-P3/CC, and sputtered Pt/CC, respectively, and their corresponding photovoltaic parameters are summarized in Table 1. The DSSC with bare CC shows a poor overall light-to-electricity conversion efficiency (η) of 0.48 ± 0.11%. After the decoration of GHBs on CC (i.e., GHBs/CC), the η was greatly enhanced to 6.20 ± 0.06%. This enhancement stems from the fact that the strain-induced structural defects on the highly curved GHBs could beneficially act as active sites for the electrocatalytic reaction at CE [38]; meanwhile, the hollow structure of GHBs provided bifacial electrocatalytic surfaces to facilitate the charge transfer from CE to electrolytic I_3^-. By using an N-GHBs-P3/CC CE, the η of the corresponding DSSC could be further improved to 7.53 ± 0.06%, comparable to 7.70 ± 0.14% of the sputtered Pt/CC CE-based cell. Obviously, by incorporating heteroatomic N, the performance of GHBs has been enhanced significantly by a 21% increase in the cell efficiency. Besides, different efficiency of a DSSC, by using a CE of GHBs/CC or N-GHBs-P3/CC, is caused mainly by the variations of the short-circuit photocurrent density (J_{SC}) and fill factor (FF) of the cell. With the same photoanode and electrolyte in a DSSC, a high J_{SC} is ascribed to the good electrocatalytic ability of CE for quickly reducing the I_3^- ions, which in turn can lead to the fast charge-transfer kinetics in the cell and result in a high FF. These mechanisms will be further discussed and verified later through
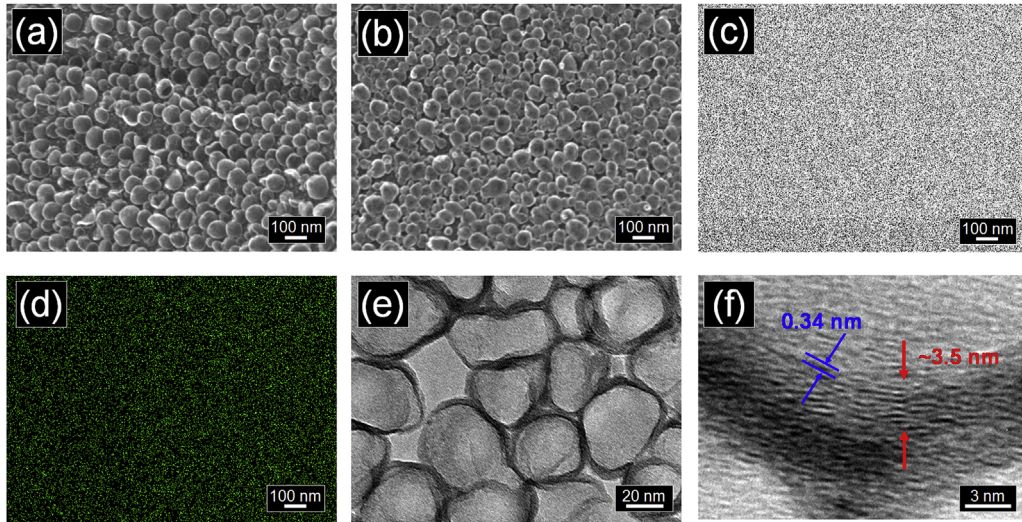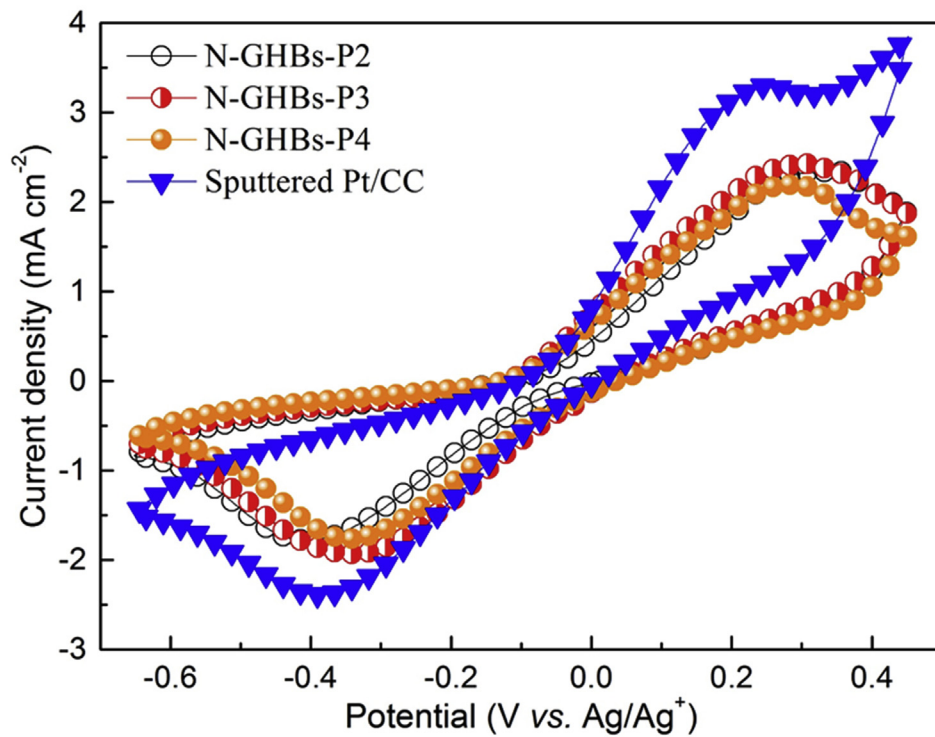
Fig. 2. The SEM images of (a) GHBs/CC and (b) N-GHBs/CC. The elemental mappings of (c) C and (d) N at their K atomic orbitals in N-GHBs/CC. (e) A TEM image of N-GHBs with hollow spherical structure. (f) HRTEM image of N-GHBs with ~3.5 nm-thick graphitic layers. The electron microscopy images and elemental mappings of N-GHBs were all taken from the N-GHBs-P3 sample.

Electrodes	J_{PC} (mA cm^{-2})	$\triangle E_P$ (mV)
N-GHBs-P2/CC	-1.55	570
N-GHBs-P3/CC	-1.68	550
N-GHBs-P4/CC	-1.36	660
Sputtered Pt/CC	-1.58	530

Fig. 3. The cyclic voltammograms and electrochemical parameters of different N-GHBs/CC electrodes and sputtered Pt/CC were measured to investigate the electrochemical parameters of various N-doped states.
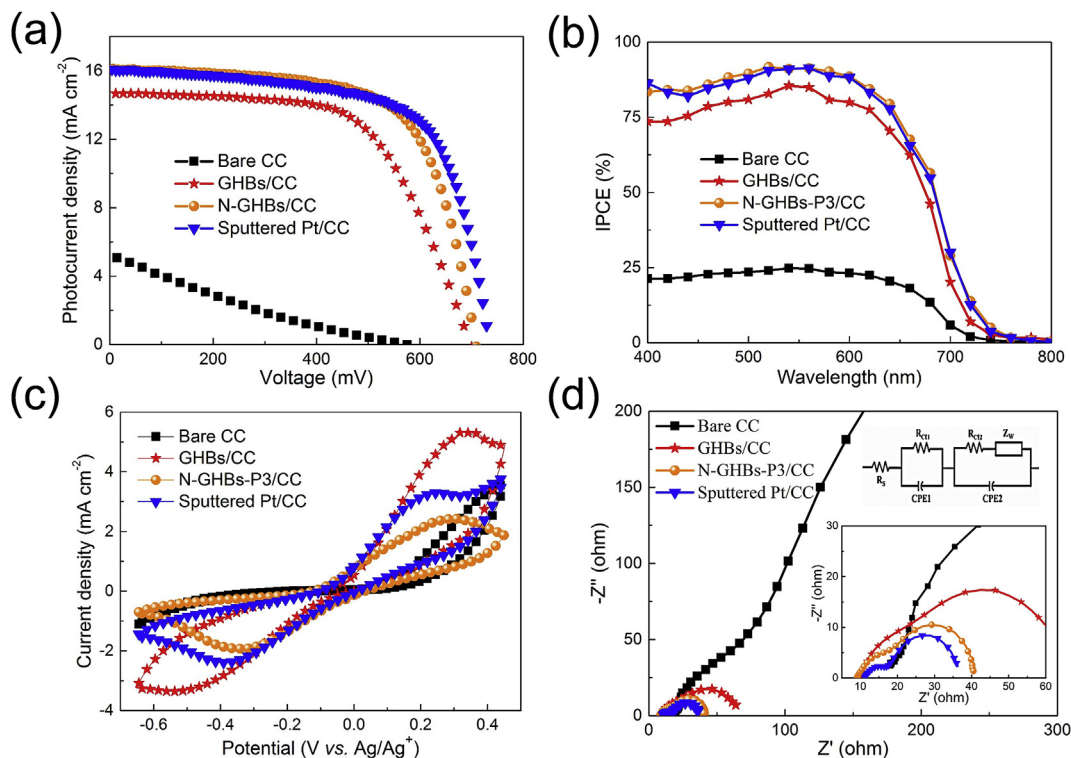
Fig. 4. The (a) photocurrent density—voltage (J—V, under AM 1.5G illumination at 100 mW cm^{-2}) curves, (b) incident photon-to-electron conversion efficiency (η) curves, (c) cyclic voltammograms, and (d) electrochemical impedance spectra (EIS, under AM 1.5G illumination at 100 mW cm^{-2}) of various CEs (including bare CC, GHBs/CC, N-GHBs-P3/CC, and sputtered Pt/CC)-based DSSCs were investigated.

Table 1
Photovoltaic parameters of the DSSCs with various counter electrodes were measured under AM 1.5G (100 mW cm^{-2}) illumination.

Counter electrodes	η (%)	V_{OC} (mV)	J_{SC} (mA cm^{-2})	FF	J_{IPCE} (mA cm^{-2})
Bare CC	0.48 ± 0.11	571 ± 2	4.33 ± 0.83	0.19 ± 0.01	4.14
GHBs/CC	6.20 ± 0.06	697 ± 5	14.50 ± 0.27	0.61 ± 0.01	14.29
N-GHBs-P3/CC	7.53 ± 0.06	703 ± 5	16.09 ± 0.18	0.67 ± 0.01	15.99
Sputtered Pt/CC	7.70 ± 0.14	735 ± 13	15.87 ± 0.32	0.66 ± 0.01	15.77

Note: The standard deviation for each measured value is based on three DSSCs. The J_{IPCE} values were calculated from the IPCE spectra with AM 1.5G solar spectrum.

the tests by both cyclic voltammetry and electrochemical impedance spectroscopy (EIS).

Fig. 4b shows the measured incident photo-to-electron conversion efficiency (IPCE) curves of these four CEs (i.e., bare CC, GHBs/CC, N-GHBs-P3/CC, and sputtered Pt/CC)-based DSSCs. All of these DSSCs exhibit broad IPCE curves, covering most of the visible region from 400 to 800 nm, and their calculated photocurrent densities (J_{IPCE}) by integrating IPCE with the AM 1.5G solar spectrum are summarized in Table 1. These J_{IPCE} values are consistent with the corresponding J_{SC} values obtained from their photovoltaic performances (Fig. 4a and Table 1).

Fig. 4c displays the cyclic voltammograms of the four CEs tested and their corresponding J_{PC} and ΔE_P values are listed in Table S1 of the Supporting Information. As shown in Table S1, the J_{PC} relating to the reduction of the I$_3^-$ ions follows an order of N-GHBs-P3/CC (-1.68 mA cm^{-2}) > sputtered Pt/CC (-1.58 mA cm^{-2}) » GHBs/CC (-0.96 mA cm^{-2}) » bare CC; the ΔE_P for the redox reaction of the I$^-$/ I$_3^-$ ions follows an order of sputtered Pt/CC (530 mV) < N-GHBs-P3/ CC (550 mV) « GHBs/CC (710 mV) « bare CC. Among the carbon-based electrodes (i.e., bare CC, GHBs/CC, and N-GHBs-P3/CC), N-GHBs-P3/CC exhibits the largest J_{PC} and the smallest ΔE_P, indicating the best charge-transfer kinetics in N-GHBs-P3/CC and echoing the highest J_{SC} and FF of the corresponding DSSC, consequently leading

to the highest η. Despite a lower $k°$ due to the larger ΔE_P, N-GHBs-P3/CC shows a higher J_{PC} than the sputtered Pt/CC because of the larger surface area of N-GHBs-P3 [24,35,36]. Therefore, as listed in Table 1, a DSSC with the N-GHBs-P3/CC CE exhibits a comparable η (7.53 ± 0.06%) to that (7.70 ± 0.14%) of the sputtered Pt/CC CE-based cell.

Finally, EIS was employed to study the charge-transfer resistances in DSSCs. As shown in Fig. 4d, the EIS spectra of the DSSCs with bare CC, GHBs/CC, N-GHBs-P3/CC, and sputtered Pt/CC CEs were measured under AM 1.5G (100 mW cm^{-2}) illumination. An equivalent circuit depicted in the upper inset is adopted to estimate the resistance of each interface in a DSSC. Basically, the EIS spectrum of a DSSC shows three semicircles in the frequency range of 10 mHz—100 kHz. While the first and second semicircles correspond to the charge-transfer resistance at the CE/electrolyte (R_{ct1}) and at the TiO$_2$/dye/electrolyte interface (R_{ct2}), respectively, the third corresponds to the Warburg diffusion resistance (Z_W) of the I$^-$/I$_3^-$ ions in electrolyte. Z_W virtually overlaps with R_{ct2} due to the short length for the diffusion of the I$^-$/I$_3^-$ ions available with the thin spacer used (i.e., 60 μm—thick Surlyn® film), in addition, owing to the low viscosities of the solvents used in our electrolytes (e.g., 0.37 and 1.60 cp for acetonitrile and 3-methoxypropionitrile, respectively) [39—41]. The values of R_{ct1} (listed in Table S2 of the

Supporting Information) are 70.65, 23.42, 10.73, and 7.57 Ω for the DSSCs with bare CC, GHBs/CC, N-GHBs-P3/CC, and sputtered Pt/CC CEs, respectively. For a DSSC, with a lower R_{ct1}, representing the less loss of internal energy at the interface between CE and electrolyte during the electrocatalytic process, the reduction reaction of I_3^- (i.e., $I_3^- + 2e^- \rightarrow 3I^-$) can work more efficiently at CE, followed by the better regeneration of the oxidized dye. Therefore as shown in Table S2, the R_{ct2}, which is relating to the charge-transfer resistance at the TiO_2/dye/electrolyte interface, follows an order of sputtered Pt/CC (18.53 Ω) < N-GHBs-P3/CC (21.23 Ω) < GHBs/CC (31.98 Ω) ≪ bare CC (1278 Ω). After examining these R_{ct} values, we confirmed that the lower charge-transfer resistances are responsible for the greater performance of DSSCs.

3. Conclusions

We developed a one-step CVD method to synthesize all-carbon N-GHBs/CC CEs as an alternative to Pt used in DSSCs. The CVD-synthesized 3D spherical structure of GHBs with a high N-doping content (12.1%) has significantly enhanced the catalytic activity toward the I^-/I_3^- redox reaction. The photovoltaic performance of 7.53% achieved by the N-GHBs-P3/CC CE is comparable to 7.70% of a standard sputtered Pt CE, which is attributed to an increase of the specific surface area and a decrease of the charge-transfer resistance. Moreover, the as-synthesized N-GHBs with different N-doped states could be controlled simply by adjusting the evaporation rate of the melamine precursor. The contents of pyridinic N and quaternary N in N-GHBs/CC CEs have been demonstrated to play a crucial role in the catalytic activity in DSSCs. With a better understanding of the N-doped states in graphene, a guideline can be developed for designing highly efficient carbon-based electrocatalysts for economical DSSCs.

Conflict of interest

The authors declare no competing financial interests.

Acknowledgment

Appendix A. Supplementary data

Supplementary data related to this article can be found at https://doi.org/10.1016/j.mtener.2018.02.006.

References

[1] B. O'Regan, M. Grätzel, A low-cost, high-efficiency solar-cell based on dye-sensitized colloidal TiO₂ films, Nature 353 (1991) 737–740.

[2] A. Yella, H.W. Lee, H.N. Tsao, C. Yi, A.K. Chandiran, M.K. Nazeeruddin, E.W.G. Diau, C.Y. Yeh, S.M. Zakeeruddin, M. Grätzel, Porphyrin-sensitized solar cells with cobalt(II/III)–based redox electrolyte exceed 12 percent efficiency, Science 171 (2002) 162–171.

[3] S. Yun, A. Hagfeldt, T. Ma, Pt-free counter electrode for dye-sensitized solar cells with high efficiency, Adv. Mater. 26 (2014) 6210–6237.

[4] B.E. Hardin, H.J. Snaith, M.D. McGehee, The renaissance of dye-sensitized solar cells, Nat. Photon. 6 (2012) 162–169.

[5] X. Cai, S. Hou, H. Wu, Z. Lv, Y. Fu, D. Wang, C. Zhang, H. Kafafy, Z. Chu, D. Zou, All-carbon electrode-based fiber-shaped dye-sensitized solar cells, Phys. Chem. Chem. Phys. 14 (2012) 125–130.

[6] L. Kavan, J.H. Yum, M.K. Nazeeruddin, M. Grätzel, Graphene nanoplatelet cathode for Co(III)/(II) mediated dye-sensitized solar cells, ACS Nano 5 (2011) 9171–9178.

[7] X. Cui, J. Xiao, Y. Wu, P. Du, R. Si, H. Yang, H. Tian, J. Li, W.H. Zhang, D. Deng, X. Bao, A graphene composite material with single cobalt active sites: a highly

[8] C.C. Chen, C.J. Kuo, C.D. Liao, C.F. Chang, C.A. Tseng, C.R. Liu, Y.T. Chen, Growth of large-area graphene single crystals in confined reaction space with diffusion-driven chemical vapor deposition, Chem. Mater. 27 (2015) 6249–6258.

[9] C.D. Liao, Y.Y. Lu, S.R. Tamalampudi, H.C. Cheng, Y.T. Chen, Chemical vapor deposition synthesis and Raman spectroscopic characterization of large-area graphene sheets, J. Phys. Chem. A 117 (2013) 9454–9461.

[10] P.Y. Chen, C.T. Li, C.P. Lee, R. Vittal, K.C. Ho, PEDOT-decorated nitrogen-doped graphene as the transparent composite film for the counter electrode of a dye-sensitized solar cell, Nano Energy 12 (2015) 374–385.

[11] C.A. Lin, C.P. Lee, S.T. Ho, T.C. Wei, Y.W. Chi, K.P. Huang, J.H. He, Nitrogen-doped graphene/platinum counter electrodes for dye-sensitized solar cells, ACS Photonics 1 (2014) 1264–1269.

[12] P. Zhai, C.C. Lee, Y.H. Chang, C. Liu, T.C. Wei, S.P. Feng, A significant improvement in the electrocatalytic stability of N-doped graphene nano-sheets used as a counter electrode for [Co(bpy)₃]³⁺/²⁺ based porphyrin-sensitized solar cells, ACS Appl. Mater. Interfaces 7 (2015) 2116–2123.

[13] W. Yang, X. Xu, L. Hou, X. Ma, F. Yang, Y. Wang, Y. Li, Insight into the topological defects and dopants in metal-free holey graphene for triiodide reduction in dye-sensitized solar cells, J. Mater. Chem. A 5 (2017) 5952–5960.

[14] Q. Luo, F. Hao, S. Wang, H. Shen, L. Zhao, J. Li, M. Grätzel, H. Lin, Highly efficient metal-free sulfur-doped and nitrogen and sulfur dual-doped reduced graphene oxide counter electrodes for dye-sensitized solar cells, J. Phys. Chem. C 118 (2014) 17010–17018.

[15] M. Batmunkh, A. Shrestha, G. Gao, L. Yu, J. Zhao, M.J. Biggs, C.J. Shearer, J.G. Shapter, Sulfur-doped graphene with iron pyrite (FeS₂) as an efficient and stable electrocatalyst for the iodine reduction reaction in dye-sensitized solar cells, Sol. RRL 1 (2017) 1700011.

[16] M.H. Yeh, L.Y. Lin, L.Y. Chang, Y.A. Leu, W.Y. Cheng, J.J. Lin, K.C. Ho, Dye-sensitized solar cells with reduced graphene oxide as the counter electrode prepared by a green photothermal reduction process, ChemPhysChem 15 (2014) 1175–1181.

[17] Z. Wang, P. Li, Y. Chen, J. He, J. Liu, W. Zhang, Y. Li, Phosphorus-doped reduced graphene oxide as an electrocatalyst counter electrode in dye-sensitized solar cells, J. Power Sources 263 (2014) 246–251.

[18] J.F. Chen, Y. Mao, H.F. Wang, P. Hu, Theoretical study of heteroatom doping in tuning the catalytic activity of graphene for triiodide reduction, ACS Catal. 6 (2016) 6804–6813.

[19] M.J. Ju, J.C. Kim, H.J. Choi, I.T. Choi, S.G. Kim, K. Lim, J. Ko, J.J. Lee, I.Y. Jeon, J.B. Baek, H.K. Kim, N-doped graphene nanoplatelets as superior metal-free counter electrodes for organic dye-sensitized solar cells, ACS Nano 7 (2013) 5243–5250.

[20] Y. Xue, J. Liu, H. Chen, R. Wang, D. Li, J. Qu, L. Dai, Nitrogen-doped graphene foams as metal-free counter electrodes in high-performance dye-sensitized solar cells, Angew. Chem. Int. Ed. 51 (2012) 12124–12127.

[21] J. Ma, C. Li, F. Yu, J. Chen, "Brick-like" N-doped graphene/carbon nanotube structure forming three-dimensional films as high performance metal-free counter electrodes in dye-sensitized solar cells, J. Power Sources 273 (2015) 1048–1055.

[22] Y. Chen, K. Fu, S. Zhu, W. Luo, Y. Wang, Y. Li, E. Hitz, Y. Yao, J. Dai, J. Wan, V.A. Danner, T. Li, L. Hu, Reduced graphene oxide films with ultrahigh conductivity as Li-ion battery current collectors, Nano Lett. 16 (2016) 3616–3623.

[23] X. Meng, C. Yu, X. Song, Y. Liu, S. Liang, Z. Liu, C. Hao, J. Qiu, Nitrogen-doped graphene nanoribbons with surface enriched active sites and enhanced performance for dye-sensitized solar cells, Adv. Energy Mater. 5 (2015) 1500180.

[24] S. Hou, X. Cai, H. Wu, X. Yu, M. Peng, K. Yan, D. Zou, Nitrogen-doped graphene for dye-sensitized solar cells and the role of nitrogen states in triiodide reduction, Energy Environ. Sci. 6 (2013) 3356–3362.

[25] G. Wang, W. Xing, S. Zhuo, Nitrogen-doped graphene as low-cost counter electrode for high-efficiency dye-sensitized solar cells, Electrochim. Acta 92 (2013) 269–275.

[26] H.M. Jeong, J.W. Lee, W.H. Shin, Y.J. Choi, H.J. Shin, J.K. Kang, J.W. Choi, Nitrogen-doped graphene for high-performance ultracapacitors and the importance of nitrogen-doped sites at basal planes, Nano Lett. 11 (2011) 2472–2477.

[27] Y. Wang, Y. Shao, D.W. Matson, J. Li, Y. Lin, Nitrogen-doped graphene and its biosensing, ACS Nano 4 (2010) 1790–1798.

[28] A. Gölzhäuser, C. Wöll, The formation of nitrogen-containing functional groups on carbon nanotube surfaces: a quantitative XPS and TPD study, Phys. Chem. Chem. Phys. 12 (2010) 4351–4359.

[29] W.W. Wang, J.S. Dang, X. Zhao, S. Nagase, Formation mechanisms of graphitic-N: oxygen reduction and nitrogen doping of graphene oxides, J. Phys. Chem. C 120 (2016) 5673–5681.

[30] D. Guo, R. Shibuya, C. Akiba, S. Saji, T. Kondo, J. Nakamura, Active sites of nitrogen-doped carbon materials for oxygen reduction reaction clarified using model catalysts, Science 351 (2016) 361–365.

[31] C.P. Lee, L.Y. Lin, P.Y. Chen, R. Vittal, K.C. Ho, All-solid-state dye-sensitized solar cells incorporating SWCNTs and crystal growth inhibitor, J. Mater. Chem. 20 (2010) 3619–3625.

[32] D. Wei, Y. Liu, Y. Wang, H. Zhang, L. Huang, G. Yu, Synthesis of N-doped graphene by chemical vapor deposition and its electrical properties, Nano Lett. 9 (2009) 1752–1758.

[33] D. Wei, Y. Liu, L. Cao, L. Fu, X. Li, Y. Wang, G. Yu, D. Zhu, A new method to synthesize complicated multibranched carbon nanotubes with controlled architecture and composition, Nano Lett. 6 (2006) 186–192.

[34] C.P. Lee, C.T. Li, K.C. Ho, Use of organic materials in dye-sensitized solar cells, Mater. Today 20 (2017) 267–283.

[35] W. Li, C. Tan, M.A. Lowe, H.D. Abruña, D.C. Ralph, Electrochemistry of individual monolayer graphene sheets, ACS Nano 5 (2011) 2264–2270.

[36] C.P. Lee, K.Y. Lai, C.A. Lin, C.T. Li, K.C. Ho, C.I. Wu, S.P. Lau, J.H. He, A paper-based electrode using a graphene dot/PEDOT: PSS composite for flexible solar cells, Nano Energy 36 (2017) 260–267.

[37] L. Lai, J.R. Potts, D. Zhan, L. Wang, C.K. Poh, C. Tang, H. Gong, Z. Shen, J. Lin, R.S. Ruoff, Exploration of the active center structure of nitrogen-doped graphene-based catalysts for oxygen reduction reaction, Energy Environ. Sci. 5 (2012) 7936–7942.

[38] C.A. Tseng, C.C. Chen, R.K. Ulaganathan, C.P. Lee, H.C. Chiang, C.F. Chang, Y.T. Chen, One-step synthesis of antioxidative graphene-wrapped copper nanoparticles on flexible substrates for electronic and electrocatalytic applications, ACS Appl. Mater. Interfaces 9 (2017) 25067–25072.

[39] Y. Ezhumalai, B. Lee, M.S. Fan, B. Harutyunyan, K. Prabakaran, C.P. Lee, S.H. Chang, J.S. Ni, S. Vegiraju, P. Priyanka, Y.W. Wu, C.W. Liu, S. Yau, J.T. Lin, C.G. Wu, M.J. Bedzyk, R.P.H. Chang, M.C. Chen, K.C. Ho, T.J. Marks, Metal-free branched alkyl tetrathienoacene (TTAR)-based sensitizers for high-performance dye-sensitized solar cells, J. Mater. Chem. A 5 (2017) 12310–12321.

[40] L.Y. Chang, C.T. Li, Y.Y. Li, C.P. Lee, M.H. Yeh, K.C. Ho, J.J. Lin, Morphological influence of polypyrrole nanoparticles on the performance of dye-sensitized solar cells, Electrochim. Acta 155 (2015) 263–271.

[41] L.Y. Chang, C.P. Lee, R. Vittal, J.J. Lin, K.C. Ho, Enhanced performance of a dye-sensitized solar cell with an amphiphilic polymer-gelled ionic liquid electrolyte, J. Mater. Chem. A 1 (2013) 3055–3060.

Supporting Information

One-step synthesis of graphene hollow nanoballs with various nitrogen-doped states for electrocatalysis in dye-sensitized solar cells

Chi-Ang Tseng,[a,†] Chuan-Pei Lee,[b,†] Yi-June Huang,[c] Hao-Wei Pang,[c] and Kuo-Chuan Ho[c,d,*] and Yit-Tsong Chen[a,b,*]

[a] Department of Chemistry, National Taiwan University, No. 1, Sec. 4, Roosevelt Road, Taipei 106, Taiwan

[b] Institute of Atomic and Molecular Sciences, Academia Sinica, P.O. Box 23-166, Taipei 106, Taiwan

[c] Department of Chemical Engineering, National Taiwan University, Taipei 106, Taiwan.

[d] Institute of Polymer Science and Engineering, National Taiwan University, Taipei 106, Taiwan

[*]*Address correspondence to:* kcho@ntu.edu.tw, ytcchem@ntu.edu.tw

[†] These authors contributed equally.

Materials

Lithium iodide (LiI, synthetical grade) and iodine (I_2, synthetical grade) were obtained from Merck. Acetone (99+%), Tert-butyl alcohol (tBA, 96%), guanidine thiocyanate (GuSCN, 99+%), and 4-tert-butylpyridine (TBP, 96%) were purchased from Acros. Ti (IV) tetraisopropoxide (TTIP, > 98%), lithium perchlorate ($LiClO_4$, ≥98.0%), ethanol (EtOH, absolute), isopropyl alcohol (IPA, 99.5%), sulfuric acid (H_2SO_4, 95–97%), and 2-methoxyethanol (99.95%) were received from Sigma-Aldrich. Acetonitrile (ACN, 99.99%) was obtained from J. T. Baker. 1,2-dimethyl-3-propylimidazolium iodide (DMPII) and cis-diisothiocyanato-bis (2,2'-bipyridyl-4,4'-dicarboxylato) ruthenium (II) bis(tetra-butylammonium) (N719 dye) were purchased from Solaronix (S.A., Aubonne, Switzerland). Carbon cloth (CC, W0S1002, thickness = 0.36 mm, basic weight = 120 g cm^{-2}, sheet resistance = 0.63 Ω sq.$^{-1}$) was obtained from CeTech Co., Ltd., Taiwan. Cu foils (25 µm in thickness, purity 99.8 %) were purchased from Alfa Aesar. The gases of methane (CH_4, 99.9995 %) and hydrogen (H_2, 99.9995 %) were purchased from FMI gas Co. Ltd., Taiwan.

Syntheses of N-GHBs and GHBs

The N-GHBs samples were synthesized in CVD reaction with the self-assisted catalytic growth of N-doped graphene shells on copper nanoparticles (CuNPs), in which the CuNP cores were later etched away by Marble's reagent. An illustration of the CVD system is presented in Figure 1a of the main text. The CVD system contains a temperature-programmable furnace (40 cm in length) equipped with a quartz tube of 1 inch in diameter. One end of the reaction tube was a gas inlet and the other end was evacuated with a dry pump. CH_4 and H_2 were employed as a chemical precursor and a carrier gas (both with the flow rate of 200 sccm), respectively, in the synthetic reaction of nitrogen-doped graphene hollow nanoballs (N-GHBs). Another precursor

of melamine as a nitrogen source was placed at different locations away from the furnace edge near the gas inlet. A collector substrate of carbon cloth (CC) was put inside the quartz tube and located ~3 cm away from the furnace edge near the pump. Cu foils mounted on a tungsten boat were placed at the center of the furnace. The furnace was then heated to 1090 ℃, which is higher than the melting point of Cu, resulting in the formation of CuNPs. During the synthetic reaction, the as-grown CuNPs could simultaneously catalyze the formation of graphene on their surfaces and serve as a template for the N-GHBs growth. Finally, the as-synthesized vapor-phase N-doped graphene-wrapped CuNPs were carried by the gas flow to deposit on the collector substrate for 2 hours.

The synthesis of GHBs was the same as the synthetic protocols described above, except without using melamine as a precursor.

Preparation of counter electrodes (CEs)

The CC substrates were cleaned by soaking into a H_2SO_4 solution for 1 week, and then washed sequentially with deionized water, EtOH, and IPA. The GHBs and N-GHBs were prepared separately on the cleaned CC substrates (i.e., GHBs/CC and N-GHBs/CC) for the uses of metal-free counter electrodes (CEs) in DSSCs. Meanwhile, a Pt catalytic layer was deposited on the cleaned CC substrate as a standard CE (denoted as a sputtered Pt/CC) with a direct current (DC) sputtering method.

Fabrication of DSSCs

A TiO_2 photoanode consists of a compact layer, a transparent layer, and a scattering layer on fluorine-doped SnO_2 (FTO, TEC-7, 10 Ω sq^{-1}, NSG America Inc., New Jersey, USA) conducting glass substrate. Before using the FTO, it was cleaned

with a neutral cleaner and then washed sequentially with deionized water, acetone, and IPA. Thereafter, a precursor solution containing TTIP and 2-methoxyethanol (weight ratio = 1:3) was used to obtain the compact layer (~100 nm thick) on the cleaned FTO substrate with a spin-coating method for obtaining a good mechanical contact between the conducting glass and the TiO_2 film. A transparent layer (~10 μm thick) was coated on the compact layer by a doctor blade technique with a commercial transparent TiO_2 paste (Ti-nanoxide HT/SP, average diameter of ~13 nm, Solaronix). A scattering layer (~4 μm thick) was then coated on the transparent layer with the same doctor blade technique by using a home-made scattering paste [S1]. Before the next TiO_2 coating, each layer was sintered at 500 ^{o}C for 30 min in an ambient environment. The as-prepared TiO_2 electrode was immersed in a 5×10^{-4} M N719 dye solution, containing a mixed solvent of ACN and tBA (volume ratio = 1:1), at room temperature for 24 h. Such a prepared dye-sensitized TiO_2 photoanode was coupled with a CE; these two electrodes were separated by a 60 μm-thick Surlyn$^{®}$ film (SX1170-60, Solaronix S.A., Aubonne, Switzerland). A mixture of 1.2 M DMPII, 0.35M I_2, 0.1 M GuSCN, and 0.5 M TBP in ACN/MPN (volume ratio of 8/2) was used as the electrolyte.

Measurements and instruments

The morphology of the as-prepared GHBs/CC and N-GHBs/CC were characterized by field-emission scanning electron microscopy (FESEM, JEOL JSM 7600) equipped with an energy dispersive X-ray spectrometer (EDS) for elemental composition analyses at 10 kV. High-resolution transmission electron microscopy (HRTEM) images were recorded with an FETEM (Philips Tecnai F30) operating at an accelerating voltage of 300 kV. An X-ray photoelectron spectrometer (XPS, VG Scientific ESCALAB 250) was employed for the chemical composition analysis. To

avoid the signals overlapping between the as-synthesized samples and the CC substrate, XPS analysis was also carried out for the as-synthesized sample on silicon wafer (with a 300 nm-thick SiO2 dielectric layer).

The surface of a DSSC was covered by a mask with a light-illuminating area of 0.16 cm^2 and then illuminated by a class A quality solar simulator (XES-301S, AM 1.5G, San-Ei Electric Co., Ltd.) with the light intensity of 100 mW cm^{-2}. Incident light intensity (100 mW cm^{-2}) was calibrated with a standard Si cell (PECSI01, Peccell Technologies, Inc., Yokohama, Japan). Photoelectrochemical characteristics of the DSSC were recorded with a potentiostat/galvanostat (PGSTAT 30, Autolab, Eco-Chemie, the Netherlands). Electrochemical impedance spectroscopy (EIS) analysis was performed using the above-mentioned potentiostat/galvanostat, equipped with an FRA2 module, under a constant light illumination of 100 mW cm^{-2}. The frequency range explored was 10 mHz–100 kHz. The applied bias voltage was set at the open-circuit voltage of the DSSC, between the CE and the dye-sensitized TiO_2 photoanode, starting from the short-circuit condition; the corresponding alternative current (AC) amplitude was 10 mV. Impedance spectra data were analyzed by fitting them to an equivalent circuit model, using Z-view software [S2–S4]. The incident photo-to-electron conversion efficiency (IPCE) curves were obtained at the short-circuit condition. The light source was a class A quality solar simulator (PEC-L11, AM1.5G, Peccell Technologies, Inc.); light was focused through a monochromator (model 74100, Oriel Instrument, California, USA) onto the photovoltaic cell. The monochromator was incremented through the visible spectrum to generate the IPCE (λ) as defined below,

$$IPCE\ (\lambda) = 1240\ (J_{SC}/\lambda\varphi)$$

where λ is the wavelength, J_{SC} is the short-circuit photocurrent density (mA cm^{-2}) recorded with a potentiostat/galvanostat, and φ is the incident radiative flux (W m^{-2})

measured with an optical detector (model 818-SL, Newport, California, USA) and power meter (model 1916-R, Newport, California, USA).

Cyclic voltammetry (CV) was performed to investigate the electrocatalytic abilities of CEs. The CV was carried out with a three-electrode electrochemical system, by using an electrode (e.g., one of bare CC, GHB/CC, NGHB/CC, and sputtered Pt/CC) as the working electrode, a Pt foil as the CE, and an Ag/Ag^+ electrode as the reference electrode in an ACN solution, containing 10 mM I^-, 1 mM I_2, and 0.1 M $LiClO_4$.

Deconvolution of the XPS spectra of N-GHBs-P2 and N-GHBs-P4
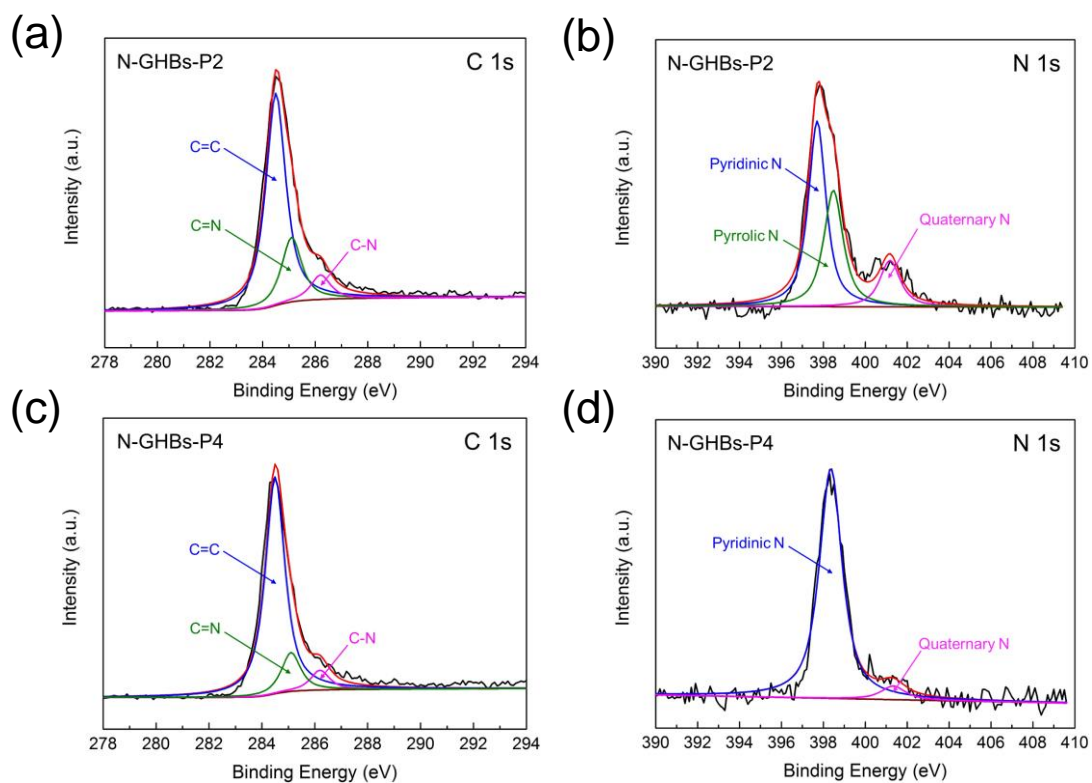

Figure S1. The deconvolution of high-resolution C1s and N1s XPS spectra for (a–b) N-GHBs-P2 and (c–d) N-GHBs-P4.

Calculation of crystallite size of graphene

Figure S2 shows the Raman spectrum of the N-GHBs-P3 sample, where the intensity ratio of the D to G bands (I_D/I_G) is inversely related to the crystallite size of graphene, which can be calculated from the Tuinstra-Koenig relationship:[S5]

$$L_a \text{ (nm)} = 2.4 \times 10^{-10} \times \lambda^4 \times (I_D/I_G)^{-1}$$

where L_a and λ are the crystallite size of graphene and the wavelength of an incident laser, respectively.

The I_D/I_G for N-GHBs-P3 was measured to be ~1.3 and the corresponding crystallite size of graphene is ~10 nm, suggesting that the N-GHBs are composed of finite crystallite size of graphene with plentiful edges.
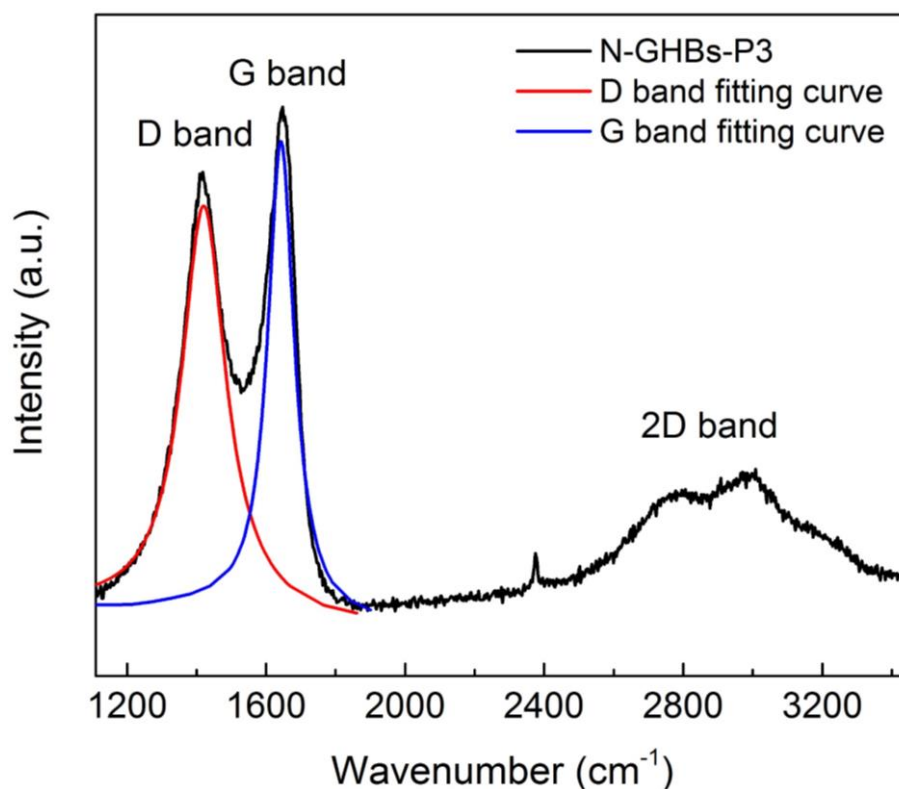

Figure S2. Raman spectrum of N-GHBs-P3 was measured with an excitation at 488 nm. The crystallite size of graphene in N-GHBs-P3 was calculated to be ~10 nm.

Electrochemical stability of sputtered Pt/CC and N-GHBs-P3/CC

To investigate the chemical stability of the electro-catalytic electrodes in the iodine/iodide electrolytes, the symmetrical dummy cells with two identical electrodes of sputtered Pt/CC and N-GHBs-P3/CC were fabricated for EIS aging measurements. In general, the EIS spectrum of a symmetrical dummy cell shows two semicircles in the measured frequency range. The first and second semicircles correspond to the charge-transfer processes occurring at the electro-catalytic electrode/electrolyte interface (R_{ct1}) and the Warburg diffusion process of the I^-/I_3^- ions in the electrolyte ($R_{diff.}$), respectively. As shown in Figure S3, the device using N-GHBs-P3/CC electrodes survived in this test without apparent changes in its EIS spectrum; in contrast, the R_{ct1} of the device using Pt/CC electrodes increased obviously. This result significantly highlights the superior electrochemical stability of the N-GHBs-P3/CC electrode in the I^-/I_3^- electrolytes.
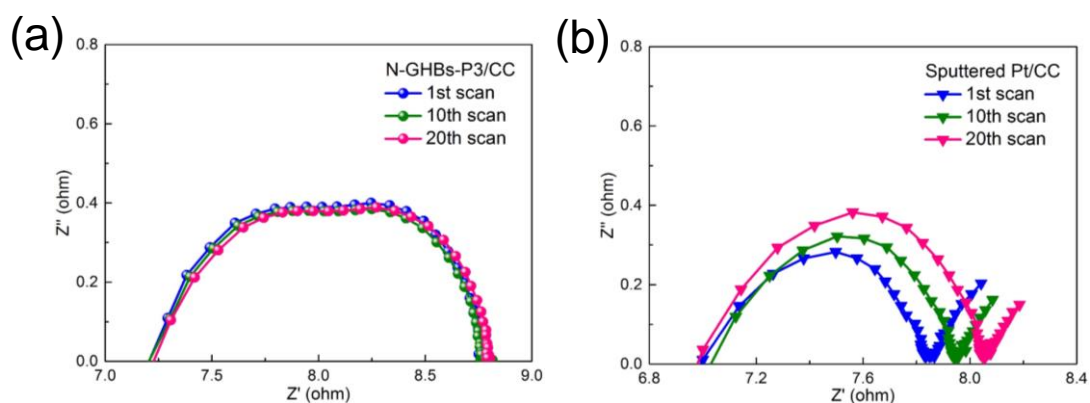

Figure S3. Electrochemical stability tests of the symmetrical dummy cells with two identical electrodes of (a) N-GHBs-P3/CC and (b) sputtered Pt/CC via EIS measurements, which were carried out consecutively at 0 V from 100 kHz to 10 mHz and repeated 20 times for each dummy cell containing the I^-/I_3^--based organic electrolytes.

Table S1. Electrochemical parameters for the cyclic voltammograms of various electrodes.

Electrodes	J_{PC} (mA cm^{-2})	ΔE_P (mV)
Bare CC	N.A.	N.A.
GHBs/CC	-0.96	710
N-GHBs-P3/CC	-1.68	550
Sputtered Pt/CC	-1.58	530

Table S2. Electrochemical impedance spectroscopy data of the DSSCs with various counter electrodes under AM 1.5G (100 mW cm^{-2}) illumination.

Counter electrodes	R_{ct1} (ohm)	R_{ct2} (ohm)
Bare CC	70.65	1278
GHBs/CC	23.42	31.98
N-GHBs-P3/CC	10.73	21.23
Sputtered Pt/CC	7.57	18.53

References

[S1] I.T. Chiu, C.T. Li, C.P. Lee, P.Y. Chen, Y.H. Tseng, R. Vittal, K.C. Ho, Nanoclimbing-wall-like $CoSe_2$/carbon composite film for the counter electrode of a highly efficient dye-sensitized solar cell: A study on the morphology control, Nano Energy 22 (2016) 594–606.

[S2] M.H. Yeh, L.Y. Lin, C.P. Lee, H.Y. Wei, C.Y. Chen, C.G. Wu, R. Vittal, K.C. Ho, A composite catalytic film of PEDOT:PSS/TiN–NPs on a flexible counter-electrode substrate for a dye-sensitized solar cell, J. Mater. Chem. 21 (2011) 19021–19029.

[S3] L.Y. Chang, C.T. Li, Y.Y. Li, C.P. Lee, M.H. Yeh, K.C. Ho, J.J. Lin, Morphological influence of polypyrrole nanoparticles on the performance of dye-sensitized solar cells, Electrochim. Acta 155 (2015) 263–271.

[S4] L.Y. Chang, C.P. Lee, C.T. Li, M.H. Yeh, K.C. Ho, J.J. Lin, Synthesis of a novel amphiphilic polymeric ionic liquid and its application in quasi-solid-state dye-sensitized solar cells, J. Mater. Chem. A 2 (2014) 20814–20822.

[S5] L.G. Caņado, K. Takai, T. Enoki, M. Endo, Y.A. Kim, H. Mizusaki, A. Jorio, L.N. Coelho, R. Magalhães-Paniago, M.A. Pimenta, General equation for the determination of the crystallite size L_a of nanographite by Raman spectroscopy, Appl. Phys. Lett. 88 (2006) 1998–2001.